Li-Farn Yang
Associate Professor,
Department of Mechanical Engineering,
National Chung-Cheng University,
Taiwan, R.O.C.
Mem. ASME

Meng-Sang Chew
Associate Professor,
Department of Mech. Engr. and Mechanics,
Lehigh University,
Bethlehem, PA 18015-3006
Mem. ASME

Jer-Nan Juang
Principal Scientist,
NASA Langley Research Center,
Hampton, VA 23681

Band-Drive Suspension Mechanism Design for Ground-Based Testing of Flexible Space Structures*

A suspension system based on a band mechanism is investigated to provide the free-free conditions for ground-based validation testing of flexible space structures. The band mechanism consists of a noncircular disk with a convex profile, preloaded by torsional springs at its center of rotation so that static equilibrium of the test structure is maintained at any vertical location; gravitational force will be directly counteracted during dynamic testing of the space structure. This noncircular disk within the suspension system can be configured to remain unchanged for test articles with different weights as long as the torsional spring is replaced to maintain the originally designed frequency parameter of W/k_s. Simulations of test articles which are modelled as lumped-parameter as well as continuous parameter systems are also presented.

1 Introduction

Satellites have generally been treated dynamically as rigid bodies during their mission operations. However, interest in orbiting very large space structures has resulted in the need to maneuver and control flexible structures. This need is driving research into both dynamic analysis and experimental verification of large flexible space structures under zero-gravity. Several large flexible space structures presently under investigation include the Mobile Satellite, the Large Deployable Reflector, the Freedom Space Station and other SDI weapon systems. These flexible space structures form the basis for much of the present need for various forms of preflight testing and analysis on the ground.

Flexible space structures, in general, experience free-free boundary conditions that are not readily replicable on earth. Yet, to conduct the testing of such space structures, special devices must be introduced. These devices must support the weight of structures without introducing any constraint forces which in turn impose boundary conditions that do not simulate the desired free-free boundary conditions in space. Several existing approaches and devices have been used or proposed for suspending low-frequency space structures for dynamic testing. Some of these, such as long cables, air pads, pneumatic/electric device, and springs, have been discussed in Ref. 1. The experimental performances of the prior four suspension systems have revealed some major inadequacies in their practical usage, which have also been presented in Ref. 1.

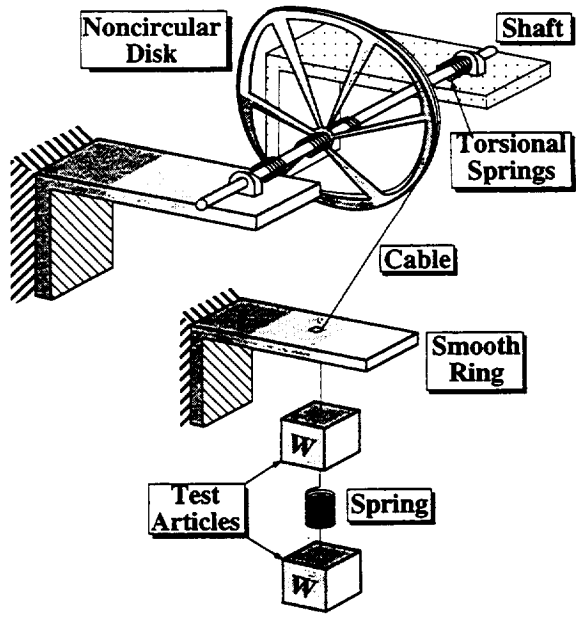

Fig. 1 Disk suspension system

Figure 1 shows a band mechanism that will be applied as a suspension system. The dynamic interaction between this system and the test article forms the basis of investigation that is reported in this paper. The system features a noncircular disk, around which a cable winds and unwinds as the disk

*Based on the Doctoral dissertation of the first author.

Contributed by the Mechanisms Committee for publication in the JOURNAL OF MECHANICAL DESIGN. Manuscript received Feb. 1993; revised March 1994. Associate Technical Editor: B. Ravani.

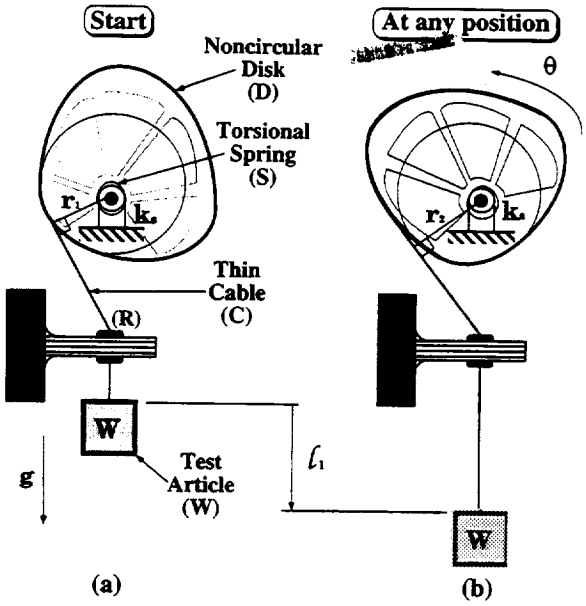

Fig. 2 Static equilibrium of a test article at two different positions under disk suspension system

rotates. This disk has a special profile designed in conjunction with the load it is to suspend, and the torsional spring stiffness chosen for the system. The torsional spring loads the disk as the disk rotates so that the torque exerted by the spring about the disk axis of rotation is exactly counterbalanced by the force exerted by the weight of the test article on the cable that winds around the disk. In this way, the suspension system is capable of keeping the test structure in static equilibrium at any vertical location so that, on a static basis, the weightless effect of a test structure in space can be simulated on earth through this suspension system. A constraint on the system is that the profile of the disk must be convex to allow the cable to wind around its edge.

Two test articles have been selected for this investigation. The first test article, which consists of two masses and one linear connecting spring, is suspended from an equilibrium position. Such a lumped-parameter system is thus treated as a simple two-degree-of-freedom discrete system whose flexibility is characterized by the connecting spring. Another test article is a flexible steel beam which is hung at its two ends in equilibrium through two identical band-drive suspension mechanisms. Simulation of the suspension system with the test articles originally at rest are carried out with excitations such as an initial displacement and an initial velocity (impulse) on the masses. The characteristics of the flexible space structures are then analyzed in conjunction with this band-drive suspension system.

2 Concept of the Band-Drive Suspension System

The problem of simulating space environments on earth inspires the development of many suspension systems that can counteract the gravitational effect on test structures in the vertical direction. A concept based on a band mechanism will be the subject of investigation as to its applicability to dynamic testing of space structures.

To begin, Figs. 2(*a*) and (*b*) show two arbitrary positions of a test article in static equilibrium suspended under this suspension device. The suspension device consists of: (*i*) a noncircular and specially profiled disk (D), (*ii*) a torsional spring (S), (*iii*) a thin cable (C), (*iv*) a smooth ring (R), and (*v*) a test article (W).

Assume that a test article is originally suspended and kept in static equilibrium at the position shown in Fig. 2(*a*) with the thin cable C wrapped around the edge of the noncircular disk D. This cable passes through the smooth frictionless ring R, and extends downward to suspend the test article W. To prevent the cable from driving the disk D and hence unwinding, a torsional spring S is attached to the axis of rotation of the disk D such that the torque exerted on the disk D, due to the load imposed by the test article W, is balanced by the torque T_{s_1} in the torsional spring S, i.e.,

$$Wr_1 = T_{s_1} \tag{1}$$

where r_1 is the moment arm which is the perpendicular distance from the disk rotational center to the cable. Then the equilibrium equation of Eq. (1) can be further written as

$$k_s(\theta_{s_0} + \theta_1) = Wr_1 \tag{2}$$

where θ_{s_0} is the angle due to the preload in the torsional spring S, and θ_1 is the rotational displacement of disk D. Note that this equation provides an explicit relationship between the angle of rotation θ_1, of the noncircular disk D, and the moment arm r_1. Suppose the test article W is displaced downward a distance of l_1 from its original equilibrium position, as shown in Fig. 2(*a*). To enable the test article W to remain in equilibrium at this new position, as illustrated in Fig. 2(*b*), the moment arm r_2 subtended at the axis of rotation of the disk D has to be larger than the moment arm r_1. This is because, to balance the increased torsional spring torque, while the cable is at the same tension W, an increase in the moment arm on the noncircular disk is needed, so that:

$$Wr_2 = T_{s_2} \tag{3}$$

In this new equilibrium position:

$$k_s(\theta_{s_0} + \theta_2) = Wr_2 \tag{4}$$

where θ_2 is new rotational displacement of disk D, as illustrated in Fig. 2(*b*). Note that the moment arms r_1, r_2 are not the radial distances to the points of tangency of the cable at the disk profile, but are the perpendicular distances from the disk rotational axis to the cable. Since the moment arm r_2 is different from r_1, it is then possible to determine the profile of the noncircular disk D such that a continuous change in the moment arm is obtained for any given position of the test article W, in such a way that when displaced from one position of static equilibrium to another position, the test article will remain in static equilibrium at this new position. That causes a weightless situation which simulates that in a space environment.

The static characteristic of the suspension system is thus governed by Eqs. (1) through (4). Obviously, the noncircular disk plays a very crucial role in such a suspension system. The profile coordinates of the noncircular disk will be derived by using envelope theory [8] in conjunction with the equilibrium equations given by Eqs. (1) through (4). This will be the subject of discussion in the following section.

3 Design of the Disk Profile

Envelope theory will be applied to generate the coordinates of the disk profile given in Fig. 3. Using kinematic inversion, as the disk rotates as observer fixed on the disk would view the sequential positions of the cable, as a sequence of straight trajectories P_0T_0, P_1T_1, P_2T_2, ..., P_nT_n as shown in Fig. 3. The swinging point, P_i ($i = 1, 2, \ldots, n$) is observed to lie on a circular path with a radius r_a, which is the distance from the rotational center O to the ring R. These straight trajectories, together when taken infinitesimally apart, give the envelope which forms the disk profile. Assuming that the initial swinging point P_0 is tangent to both the base circle O and the disk profile, the angle ϕ_0, which denotes the starting rotational position of the string, is given by:

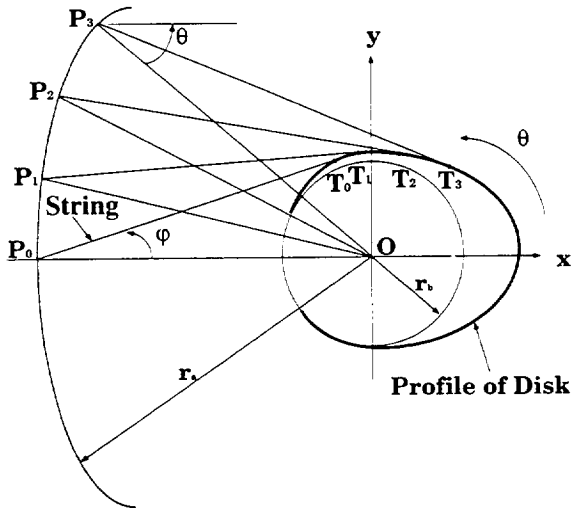

Fig. 3 Development of noncircular disk profile

$$\phi_0 = \sin^{-1}\left(\frac{r_b}{r_a}\right) \tag{5}$$

Suppose that the string is viewed by the observer at center O, while the disk rotates through an angle θ. Then the thin cable will subtend an angle of $\phi_0 + \phi$ with the vertical, at the ring. The increment angle ϕ is the rotational displacement of the string trajectory $\overline{PT}$ from its initial orientation. Therefore there exists a relationship between disk rotational angle θ and the string angular displacement ϕ. This relationship will be derived using the equilibrium Eqs. (2) and (4). From [2], a general equation of the family of lines forming the envelope is governed by a straight line which is:

$$y = mx + b \tag{6}$$

where the slope of the swinging string at the disk angular position θ is given by

$$m = \tan(\phi + \phi_0 - \theta) \tag{7}$$

and y-intercept of the string $\overline{PT}$, based on the cartesian system in Fig. 3, is

$$b = r_a \cos\theta \tan(\phi + \phi_0 - \theta) + r_a \sin\theta \tag{8}$$

This general equation of the cable $\overline{PT}$ in Eq. (7) gives a one-parameter family of strings as a function of the disk angle of rotation θ. From the theory of envelopes, an envelope of the family of the straight lines is governed by an equation:

$$F(x, y, \theta) = y - mx - b$$

$$= y - \tan(\phi + \phi_0 - \theta)[x + r_a \cos\theta] - r_a \sin\theta = 0 \tag{9}$$

Equation (9) is continuous and is a continuously differentiable function in the coordinates x and y as well as in the variable θ. Differentiating Eq. (9) with respect to the disk angle θ provides:

$$\frac{\partial F}{\partial \theta} = \tan\beta(r_a \sin\theta) - [x + r_a \cos\theta]\sec^2\beta\left(\frac{\partial \phi}{\partial \theta} - 1\right) - r_a \cos\theta = 0 \tag{10}$$

where β equals to $\phi + \phi_0 - \theta$. According to [2], the coordinates of disk profile at a given angle θ may be obtained by solving Eqs. (9) and (10), i.e.:

$$x = -r_a[A \sin\beta + \cos\theta] \tag{11}$$

where

$$A = \frac{\cos(\theta + \beta)}{\frac{\partial \phi}{\partial \theta} - 1} \tag{12}$$

Substituting Eq. (11) into Eq. (9) provides

$$y = r_a[-A \sin\beta + \sin\theta] \tag{13}$$

Initially, the angles θ and ϕ equal zero so that the starting coordinate of the noncircular disk becomes:

$$x = -2r_a \sin\left(\frac{\phi_0}{2}\right), \tag{14}$$

$$y = \frac{\sin 2\phi_0}{2} \tag{15}$$

which coincides with the point at which the starting string $\overline{P_0T_0}$ is tangent to the base circle in Fig. 3.

The rate of change of the string orientation with respect to disk rotation, $\partial\phi/\partial\theta$ can be determined by investigating the relationship between the angles ϕ and θ. Based on Eq. (2) and illustrated in Fig. 2, the equation of the initial equilibrium is governed by:

$$Wr_a \sin\phi_0 = k_s\theta_0 \tag{16}$$

For the incremental angles of θ and ϕ, from the initial orientation angles θ_0 and ϕ_0, the new equilibrium state becomes:

$$Wr_a \sin(\phi_0 + \phi) = k_s(\theta_0 + \theta) \tag{17}$$

Subtracting Eq. (16) from Eq. (17) provides:

$$Wr_a[\sin(\phi_0 + \phi) - \sin\phi_0] = k_s\theta \tag{18}$$

which can be rewritten as

$$\phi = \sin^{-1}\left[\frac{k_s\theta}{Wr_a} + \sin\phi_0\right] - \phi_0 \tag{19}$$

Differentiating Eq. (19) with respect to the angle θ yields

$$\frac{\partial \phi}{\partial \theta} = \frac{k_s}{Wr_a \cos(\phi_0 + \phi)} \tag{20}$$

Then, the profile of the noncircular disk is determined by substituting ϕ and $\partial\phi/\partial\theta$ from Eqs. (19) and (20) into the equations for the disk coordinates given by Eqs. (11) and (13). Note that the profile of the disk must be convex.

Several parameters are needed to generate the profile of the noncircular disk, and they include r_a, r_b, k_s, and W. It can readily be shown that each disk profile can be specified according to a parameter which is the ratio of the weight of the test article to the stiffness of the torsional spring, i.e., W/k_s. This means that if testing is to be conducted for another test article twice its original weight, the torsional spring stiffness must be increased by the same factor so that the same disk can again be used. Such a design, therefore, permits tremendous flexibility since different loads can be used on this device, without the need to fabricate a new disk every time a new test article with a different mass, is used.

With the disk profile design, the dynamics of the test articles can then be suspended on this band mechanism. The dynamics of these test articles in the presence of a suspension mechanism will be presented in the next section.

4 Dynamics of Test Articles and Suspension System

In simulating the test experiments of flexible space structures, the test article may be modeled as a discrete or a continuous parameter system. Two models of a test article will be considered: a lumped-parameter model and a continuous parameter flexible steel beam. In the lumped-parameter model, the test article will be modelled as two masses and a connecting linear spring suspended in equilibrium as shown in Fig. 4(*b*). Such a lumped-parameter system is thus treated as a simple two-degree-of-freedom discrete system whose flexibility is characterized by the connecting spring. In the continuous parameter model, a flexible steel beam is hung at its two ends and is suspended through two identical disk suspension systems, as shown in Fig. 5. Simulation of the ground-based

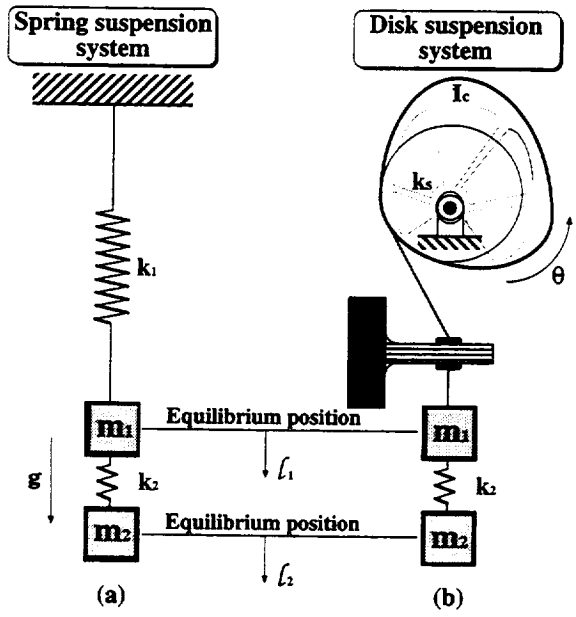

Fig. 4 A lumped-parameter model

validation testing will be implemented by providing the test article, originally in equilibrium, with the excitations such as an initial displacement or an initial velocity (impulse). The characteristics of flexible space structures are then analyzed together with the band mechanism suspension system.

4.1 Case 1: A Lumped-Parameter Model of a Test Article. The flexible space structures can be discretized into a series of lumped-parameter elements. The first test structure in Fig. 4(*b*) illustrates a discrete lumped-parameter system which approximates a flexible structure through the use of two masses and one connecting spring. The band-drive suspension system is connected to one of the masses, m_1. Notice that the weight W in Eqs. (16)–(20) stands for the weight due to the sum of the two masses, so that care is needed while developing the profile of the noncircular disk for this test article. A derivation of the dynamic equations will be discussed below.

Assume that m_1 and m_2 are the masses of the two rigid bodies, k_2 the spring stiffness between the two bodies, I_c the moment inertia of the disk, k_s the torsional spring rate and, r_a the distance between rotational center O and the ring R. Furthermore, the displacements of the two masses are denoted by l_1 and l_2, respectively, while θ and $\dot{\theta}$ denote the angular displacement and angular velocity of the noncircular disk, and ϕ is the displacement angle of the cable. Then from Fig. 4(*b*), the static equilibrium of the test article at any position is governed by

$$W=(m_1+m_2)g=\frac{k_s(\theta+\theta_0)}{r_a\sin(\phi+\phi_0)}=\frac{k_s\theta_0}{r_a\sin\phi_0} \tag{21}$$

and

$$m_2g=k_2l_{s_1} \tag{22}$$

where l_{s_1} indicates the static elongation of the spring, θ_0 is the preloaded angle of torsional spring, and ϕ_0 denotes the initial angular position of the cable. Note that the linear displacement l_1 of mass m_1 must be consistent with disk angle θ since the suspension cable is directly connected to mass m_1. Due to the convexity of disk profile, the displacement l_1, in Fig. 3, can be equated by integrating along the curvilinear path of the disk profile through the rotation θ so that:

$$l_1=\int_0^{\theta} r_a\sin(\phi+\phi_0)d\theta=\frac{k_s\left(\frac{\theta^2}{2}+\theta_0\theta\right)}{W} \tag{23}$$

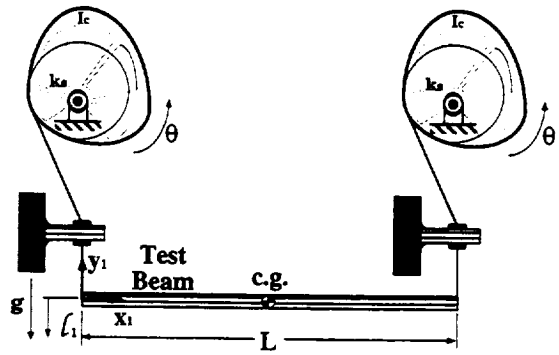

Fig. 5 A flexible steel beam

Note that the displacement l_1 of mass m_1 is a quadratic function of the disk angle θ. In fact, Eq. (23) shows a function generator which generates a parabolic curve of the displacement l_1 in terms of θ. Moreover, differentiating Eq. (23) with respect to time yields

$$\dot{l}_1=\left[\frac{k_s(\theta+\theta_0)}{W}\right]\dot{\theta} \tag{24}$$

which gives the velocity relation between $\dot{l}_1$ and $\dot{\theta}$. Therefore, the displacement and velocity of mass m_1 can be replaced by the disk angle and angular velocity through the use of Eqs. (23) and (24).

Applying Lagrange's equation of motion [3], the Lagrangian function for this system is given by

$$\hat{L}=T-V \tag{25}$$

where the kinetic energy T and the potential energy V are:

$$T=\frac{1}{2}\left\{I_c\dot{\theta}^2+m_1\left[\frac{k_s(\theta+\theta_0)}{W}\right]^2\dot{\theta}^2+m_2\dot{l}_2^2\right\}, \tag{26}$$

$$V=\frac{k_s(\theta+\theta_0)^2}{2}+\frac{k_2}{2}\left[\frac{k_s\left(\frac{\theta^2}{2}+\theta_0\theta\right)}{W}-l_2-l_{s_1}\right]^2 - m_1gk_s\left(\frac{\theta^2}{2}+\theta_0\theta\right) \tag{27}$$

Based on the Lagrangian from Eq. (25), the dynamic equation of motion in matrix form may be written in the following form:

$$\mathbf{M}\ddot{\xi}+\mathbf{K}\xi=\mathbf{f} \tag{28}$$

where ξ denotes the state vector $[\theta\ l_2]^T$. The inertia, stiffness matrices, and nonlinear force vector become

$$\mathbf{M}=\begin{bmatrix} I_c+m_1\left[\frac{k_s(\theta+\theta_0)}{W}\right]^2 & 0 \\ 0 & m_2\end{bmatrix}, \tag{29}$$

$$\mathbf{K}=\begin{bmatrix} k_s+\frac{k_sk_2}{W}\left(\frac{k_s\theta_0^2}{W}-l_{s_1}\right) & -\frac{k_sk_2\theta_0}{W} \\ -\frac{k_sk_2\theta_0}{W} & k_2\end{bmatrix}, \tag{30}$$

$$\mathbf{f}=[f_1\quad f_2]^T, \tag{31}$$

where

$$f_1=\frac{m_1gk_s(\theta+\theta_0)}{W}-k_s\theta_0+\frac{k_sk_2}{W}\left\{\theta l_2+l_{s_1}\theta_0-\frac{k_s\theta^3}{2W}-\frac{3k_s\theta_0\theta^2}{2W}\right\} - m_1(\theta+\theta_0)\left(\frac{k_s}{W}\right)^2\dot{\theta}^2$$

and

$$f_2 = \frac{k_s k_2 \theta^2}{2W}$$

The characteristics of such a lumped-parameter model may then be observed with different initial conditions placed on the lumped masses. For comparison purposes, the dynamic responses of the same test article will be re-simulated using the soft spring suspension system shown in Fig. 4(*a*). The stiffness of the soft spring has been chosen to be equivalent to the torsional spring rate in the disk suspension system, i.e., $k_1 = k_s/r_b^2$. The governing linear dynamic equation for the suspension system in Fig. 4(*a*) can be found in [4] and will not be included in this paper. A second model of the test article is based on a continuous parameter system. The second model will be the subject of investigation in the section below.

4.2 Case 2: Flexible Steel Beam: (A Continuous—Parameter Model). The band mechanism suspension system may be applied for the dynamic testing of continuous parameter models of flexible structures as well. Figure 5 demonstrates a uniform rectangular cross-section steel beam hung on two identical disk suspension systems at its two ends. Testing of such a flexible beam is aimed at flexural vibrational behavior. Assume that the total weight of the flexible beam in static equilibrium is evenly suspended by two identical disk suspension systems. Then, the profile of the noncircular disk is developed using half the weight of the flexible beam when Eqs. (18) and (20) are applied.

Assume that the rigidity of the flexible beam is given by EI product, its density ρ, the length L, and the displacement of the beam at the left end is denoted by l_1. The local coordinates $x_1 - y_1$ are located at the left end of the flexible beam for determining the local deflection of the beam. Modal analysis technique [5, 6] will be applied to discretize the beam deflection into a series of flexural modes. The flexible beam deflects during bending vibration about its deformed static equilibrium shape, which is caused by gravity. As will be seen in the simulation of the beam behavior, only odd modes will be excited so that the flexural deflection of this floating hinged-hinged beam in the coordinates $x_1 - y_1$ is symmetrical about its center of this floating gravity. A setup of such a system is shown in Fig. 5.

The displacements and velocities of the flexible beam at two ends can be substituted by the disk angle θ and angular velocity $\dot{\theta}$ in Eqs. (23) and (24) derived in the lumped-parameter system. For the flexible beam, as shown in Fig. 5, the kinetic energy T and the potential energy V can be expressed as:

$$2T = 2I_c\dot{\theta}^2 + \int_0^L \rho[\dot{l}_1 - \dot{y}_1]\cdot[\dot{l}_1 - \dot{y}_1]dx_1 \tag{32}$$

$$2V = 2k_s[\theta + \theta_0]^2 + \int_0^L EI\left\{\frac{\partial^2 y_1}{\partial x_1 \partial x_1}\right\}^2 dx_1 \tag{33}$$

Moreover, the distributed coordinates are expanded in a orthogonal basis of assumed mode shapes so that:

$$y_1(x_1, t) = \psi^{\mathrm{T}}(x_1)\mathbf{q}(t), \text{ and } \begin{cases}\psi^{\mathrm{T}} = [\psi_1, \ldots, \psi_n]; \\ \mathbf{q}^{\mathrm{T}} = [q_1, \ldots, q_n]\end{cases} \tag{34}$$

where $\psi(x_1)$ is a vector of assumed mode shapes relative to spatial coordinates derived from the hinged-hinged boundary condition problem, $\mathbf{q}(t)$ is a generalized coordinate vector [5, 6], and n is the number of assumed modes.

Inserting Eq. (34) into Eqs. (32) and (33) yields

$$2T = 2I_c\dot{\theta}^2 + \rho L\,\dot{l}_1^2 + \sum_{i=1}^{n}\sum_{j=1}^{n} m_{ij}\dot{q}_i\dot{q}_j - 2\sum_{i=1}^{n} h_i\dot{q}_i\dot{l}_1, \tag{35}$$

$$2V = 2k_s[\theta + \theta_0]^2 + \sum_{i=1}^{n}\sum_{j=1}^{n} \kappa_{ij}q_iq_j \tag{36}$$

where

$$m_{ij} = \int_0^L \rho\psi_i(x_1)\psi_j(x_1)dx_1, \quad h_i = \int_0^L \rho\psi_i(x_1)dx_1,$$

$$\kappa_{ij} = \int_0^L EI\,\frac{\partial^2\psi_i}{\partial x_1\partial x_1}\,\frac{\partial^2\psi_j}{\partial x_1\partial x_1}\,dx_1 \quad \text{for } i, j = 1, 2, \ldots, n$$

Therefore, the Lagrangian for the system, as given by Eq. (25), can then be obtained. From Eqs. (35) and (36), the displacement and velocity at the beam ends are converted into the angular displacement and angular velocity of the disk. To simplify the state variables in the above equations, denote $\xi_0 = 0$, $\xi_i = q_i$, for $i = 1, 2, \ldots, n$. Using the Lagrange's equations of motion [3], the equation of motion of the system may be written in the same way as Eq. (28), where the state vector $\xi^T = [\theta, q_1, q_2, \ldots, q_n]$, and the inertia matrix $\mathbf{M}$, the stiffness matrix $\mathbf{K}$, and the nonlinear force vector $\mathbf{f}$ are given by:

$$\mathbf{M} = \begin{bmatrix} 2I_c + 4\rho L\left(\frac{k_s}{W}\right)^2[\theta + \theta_0]^2 & -\frac{2k_s[\theta + \theta_0]\mathbf{h}^T}{W} \\ -\frac{2k_s[\theta + \theta_0]\mathbf{h}}{W} & \rho L\hat{I} \end{bmatrix}, \tag{37}$$

$$\mathbf{K} = \mathrm{Diag}[0, \rho L\omega^2]; \quad \omega = \mathrm{Diag}[\omega_1, \ldots, \omega_n], \tag{38}$$

$$\mathbf{f} = \begin{bmatrix} -4\rho L\left(\frac{k_s}{W}\right)^2[\theta + \theta_0]\dot{\theta}^2 \\ 2k_s\dot{\theta}^2\mathbf{h} \end{bmatrix} \tag{39}$$

where $\hat{I}$ is an $n \times n$ identity matrix and ω_i ($i = 1, \ldots, n$) is the modal frequencies associated with the hinged-hinged shape functions $\psi_i(x_1)$ used in discretizing the deflection of the flexible beam.

5 Simulation Results

The dynamics of test articles have been derived in the previous section, and they include a lumped-parameter system as well as a continuous-parameter system. For each test article, two different excitations to the system will be implemented. The first is with an initial displacement and the second with an initial velocity, with a total of four simulations to verify the feasibility of this disk suspension system. A soft spring will be employed as a suspension system [see Fig. 4(*a*)] for the lumped-parameter system, and its simulations are then compared to those on the disk suspension system.

A convex profile of the noncircular disk is constructed by evaluating Eqs. (11) and (13). Figure 6 shows the resulting profile of the noncircular disk, with spokes used to minimize its moment of inertia. The disk radius varies from 3.0 inches to 9.5 inches. Within the disk thickness, a groove has been cut along the edge of the disk for winding the cable. The range of disk rotation based on the constructed profile is approximately 200 degrees. Such a noncircular disk, as shown in Fig. 6, will be used to implement the following dynamic simulations.

5.1 Simulations of the Lumped—Parameter Model. The model parameters of a lumped-parameter system are given as: $r_a = 12$ in, $r_b = 6$ in, $k_s = 0.5$ lb/rad, $I_c = 0.01$ lb $-$ in^2, $m_1 = m_2 = 12$ lb, and $k_2 = 1$ lb/in. Two kinds of suspension systems, a band mechanism and a spring suspension system, will be used. In the first simulation, -0.2 inch and 0.2 inch of initial displacements are specified to masses #1 and #2, respectively, but with no initial velocity. Figures 7(*a*)–7(*f*) are the simulation results of the two suspension systems. The results associated with the disk suspension system are indicated by a solid line, while those of the spring suspension system are indicated by a dotted line. Figures 7(*a*) and 7(*b*) show the angular displacement and angular velocity of the disk, re-

spectively, of the disk suspension system. Both angular displacement and angular velocity fluctuate with the natural frequency of the test article. The displacement and velocity of mass #1 are respectively shown in Figs. 7(*c*) and 7(*d*), while the displacement and velocity of mass #2 are given in Figs. 7(*e*) and 7(*f*), respectively. All the trajectories of masses #1 and #2 represent pure oscillatory motions about their equilibrium positions. The cable which connects the test article to the disk is found to be always in tension. It can be seen that there is no difference between disk suspension system and the simple spring system under specifications of initial displacements. The spring in the spring system may be too soft due to the equivalent relationship, $k_1 = k_s/r_b^2$, so that it may not be able to suspend heavy test articles. The spring stiffness for this spring suspension system cannot be arbitrarily increased because that will distort the natural frequency of the test article. The initial-displacement results provide an insight in verifying the validity of a disk suspension system when compared to the conventional spring suspension system. It also shows that the results correspond to the anticipated vibrational characteristics of mass #1 and #2 in space.

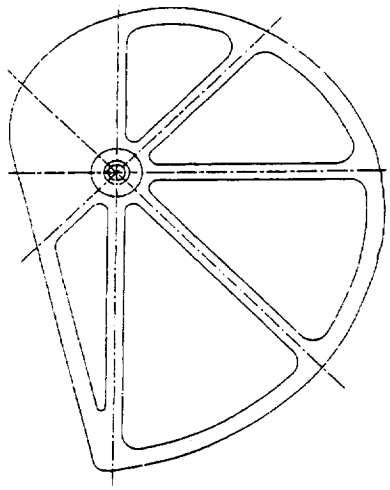

Fig. 6 Profile of noncircular disk

The second simulation of a lumped-parameter system deals with the dynamic response subjected to an initial velocity specification. An initial velocity of 2.0 inches per second acts on mass #2 to excite the whole system to move as if under an impulse. Figure 8(*a*) shows the dynamic history of the disk angle. It has an oscillatory motion superimposed on the dropping angular displacement trajectory. Figure 8(*b*) illustrates this oscillatory motion of the disk but with an average angular velocity of 9.5 deg/s, superimposed upon that oscillation. The displacements and velocities of masses #1 and #2 are shown in Figs. 8(*c*)-(*f*). In Figs. 8(*c*) and 8(*e*), the solid lines associated with the disk suspension system show that the entire test article is dropping at a constant velocity, while mases #1 and #2, which model the test article, are oscillating during this downward motion. This shows that with the use of this disk suspension system the impulse response indeed corresponds to that in a zero-gravity condition. Figures 8(*c*) and 8(*e*), on the other hand, show that the spring suspension system does not satisfy this anticipated motion trajectory of the test article (masses). The velocities of the masses shown in Figs. 8(*d*) and 8(*f*) confirm that the masses in the disk suspension system,

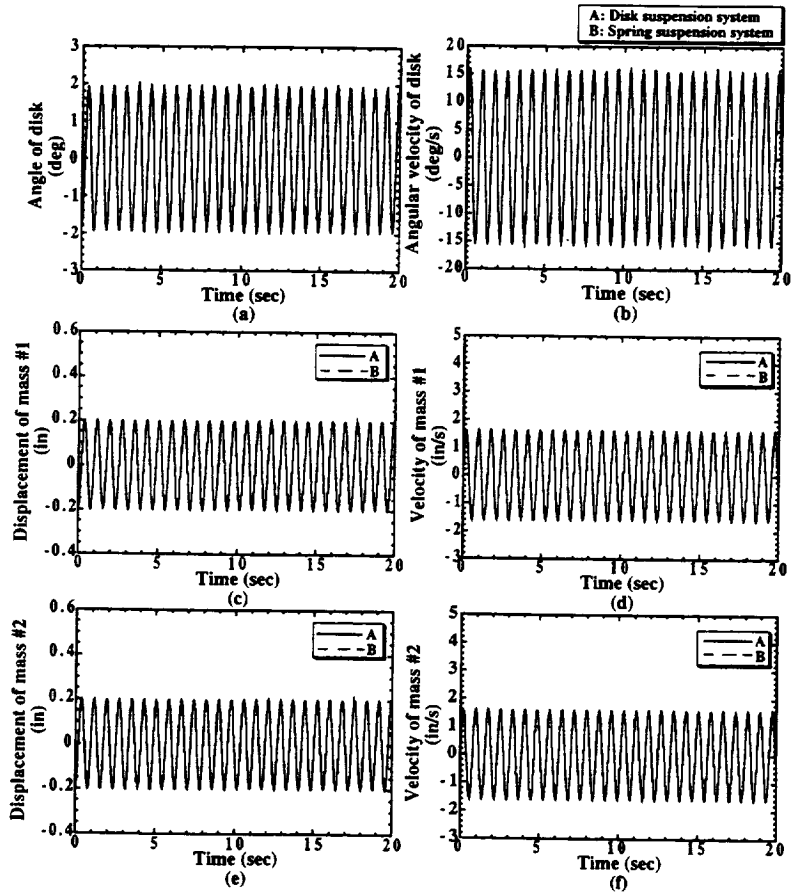

Fig. 7 Simulation results of a lumped-parameter model for the excitation of the initial displacement

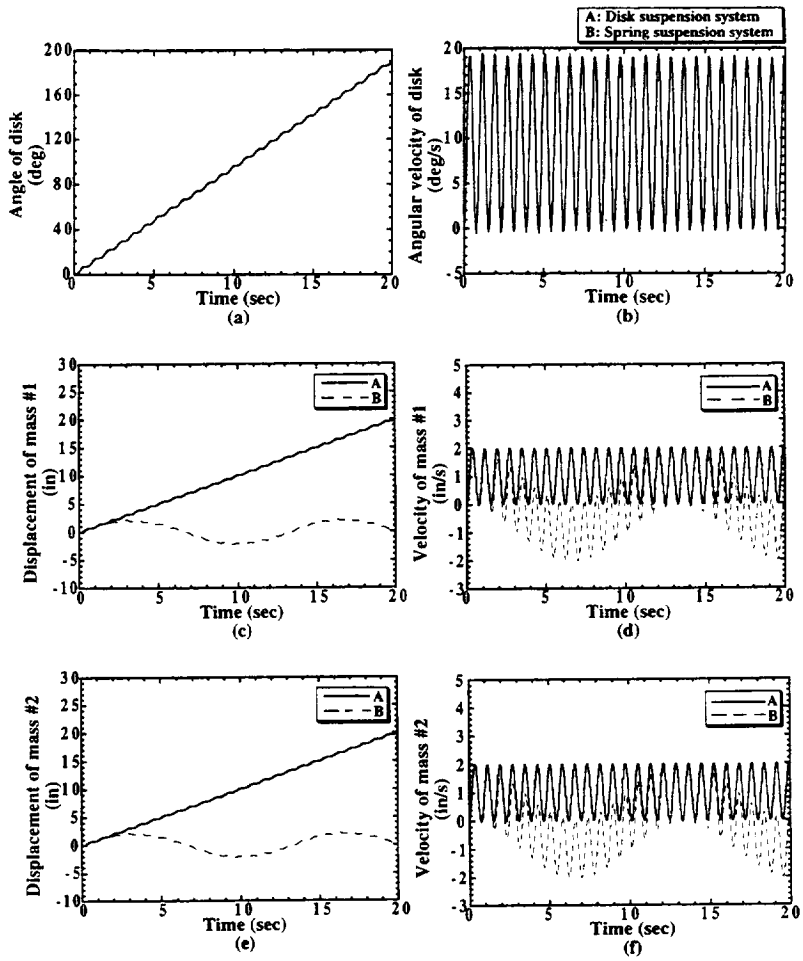

Fig. 8 Simulation results of a lumped-parameter model for the excitation of the initial velocity

on the average, do not accelerate. The pure oscillations of both the mass velocities indicate an average constant velocity of 1.0 in/s (fluctuating between 2.0 and 0.0 in/s), implying that the constant velocities are indeed due to the impulse response. This implication shows that the entire test article beneath the disk suspension system is not accelerated due to the initial impulse. Such a phenomenon is consistent with the behavior deduced from mass displacements in Figs. 8(*c*) and 8(*e*). Note that the masses oscillate at 180 degrees out of phase with each other. These figures also prove that the simple spring suspension system does not result in a correct motion for the masses in response to an initial impulse.

Figures 8(*a*)-(*f*) thus ensure that this disk suspension system is capable of simulating the dynamic behavior of the test article subjected to an impulse. The test body, accordingly, translates at a constant velocity. When the mass is imposed with an initial velocity v_0, (equivalent to an impulse) the test article will continue to travel at that same velocity, v_0, over a considerable range of travel. This is because the tension in the cable is constant and is exactly equal to the weight of the test article, so that there is no net driving force on the article during its entire range of motion. With that observation, it therefore leads to a constant velocity of the test article, and in so doing, very nearly simulates the motion of an object in space.

5.2 Simulations of the Flexible Steel Beam. In this simulation experiment, two identical disk suspension systems are employed to suspend a flexible beam that has the same weight as in the lumped-parameter model of the previous section. The model parameters of a flexible steel beam are specified by: $L = 6.562$ ft, $EI = 74.8953$ lb-ft^2, $\rho = 0.3048$ lb/in, and $h = 1.614 \times 10^{-2}$ in. Three hinged-hinged flexible modes will be assumed for the flexible steel beam. A free-free flexible beam in space has also been simulated under the same excitations for comparison with those using the disk suspension systems. In this simulation, the first and third modes will be specified with initial values. This means that the flexible beam is originally bent into a symmetric deformed configuration about its static equilibrium configuration, and then released from rest. Hence, the first and third modes are excited by this initial deformation. The simulation results are given in Figs. 9(*a*)-(*f*). Solid lines denote the results under the disk suspension systems, and dashed lines indicate those for a free-free flexible beam in space. Figures 9(*a*) and 9(*b*) show the angular displacement and angular velocity of the disk, while Figs. 9(*c*) and 9(*d*), the deflection and velocity of the beam at its center of gravity. Figures 9(*e*) and 9(*f*), on the other hand, show the deflection and velocity respectively of the beam at both ends of the beam. The odd modes, as anticipated, are very active as can be seen from results of displacement and velocity in the figures. This is due to the symmetry of the deflection about a plane through the center of gravity of the beam. In Fig. 9(*c*), the displacement at the c.g. of the beam implies that the beam oscillates about its original static equilibrium configuration during the process. It can be seen that the initial displacement response for the free-free beam in space and that suspended by disk suspension systems on the ground, superimpose. This implies that the disk suspension systems can simulate the initial

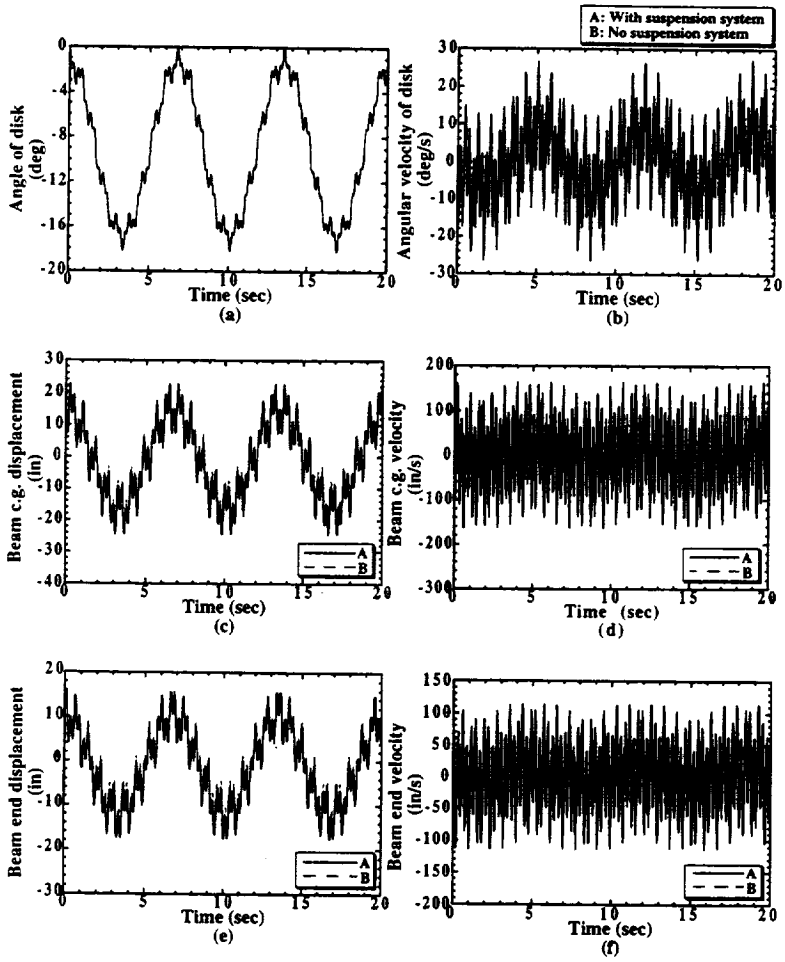

Fig. 9 Simulation results of a flexible steel beam for the excitation of the initial displacement

displacement response of the free-free flexible beam in space. Hence, the multi-mode vibration of a flexible beam can be implemented under the disk suspension system.

Finally, a fourth simulation has been conducted with the flexible beam subjected to an initial impulse. Similarly, the response of a free-free flexible beam in space is achieved by imposing the same initial impulse on the beam. Simulation results are shown in Figs. 10(*a*)-(*f*) which include the disk angle, angular velocity of disk, displacement and velocity of the c.g. of the beam, and displacements and velocities of the end points of the beam. The third mode is more pronounced in the velocity plots and the amplitude of the beam deflection at the center of gravity is larger than those at both ends. The linear slope in the oscillatory behavior in Figs. 10(*c*) and 10(*e*) indicates a constant-speed motion associated with a rigid-body mode. The flexible beam is moving upwards at a constant speed while simultaneously vibrating with respect to the local coordinates $x_1 - y_1$. The constant speed is approximately 0.7 in/sec. In fact, these impulse results of a beam imply a compound motion of the flexible space structure that includes a constant-speed rigid-body motion with flexible-body vibration superimposed on it. The results show that vibrational characteristics of a free-free flexible beam are similar with those using the disk suspension systems. The inertia of the noncircular disk may be the reason for small deviation of the impulse response in the disk suspension systems, from that in space.

The impulse response of a flexible structure has shown to be consistent in the use of this disk suspension device. The entire test structure will travel at a constant velocity with a rigid-body motion, while the traveling beam oscillates, with its flexible modes, about the moving local coordinate system. The similarities of the second and fourth simulation results validate the applicability of this disk suspension system for both discrete and continuous models.

6 Conclusion

In this article, a band mechanism design has been presented that is to be used as a ground-based suspension system to assess the characteristics of flexible space structures that operate in a weightless environment. This mechanism is characterized by a noncircular disk with a convex profile constrained into rotational motion, by a torsional spring. The suspension system is constructed to counteract the weight of the test article by using a specially constructed disk profile in conjunction with an appropriate torsional spring. The basic principle behind this suspension system is to maintain static equilibrium of the test article at any given vertical position. Envelope theory has been applied to the determination of the convex profile of the disk. It has also been shown that this suspension system is applicable for test articles with the different weights without the need to change the disk profile; the torsional spring rate has to be adjusted to maintain the static equilibrium condition of the new test article.

This mechanism has shown, under numerical simulation, to be applicable and suitable for ground-based dynamic testing of test articles, be they discrete or continuous models. Two kinds of test articles have been chosen for the simulation, a

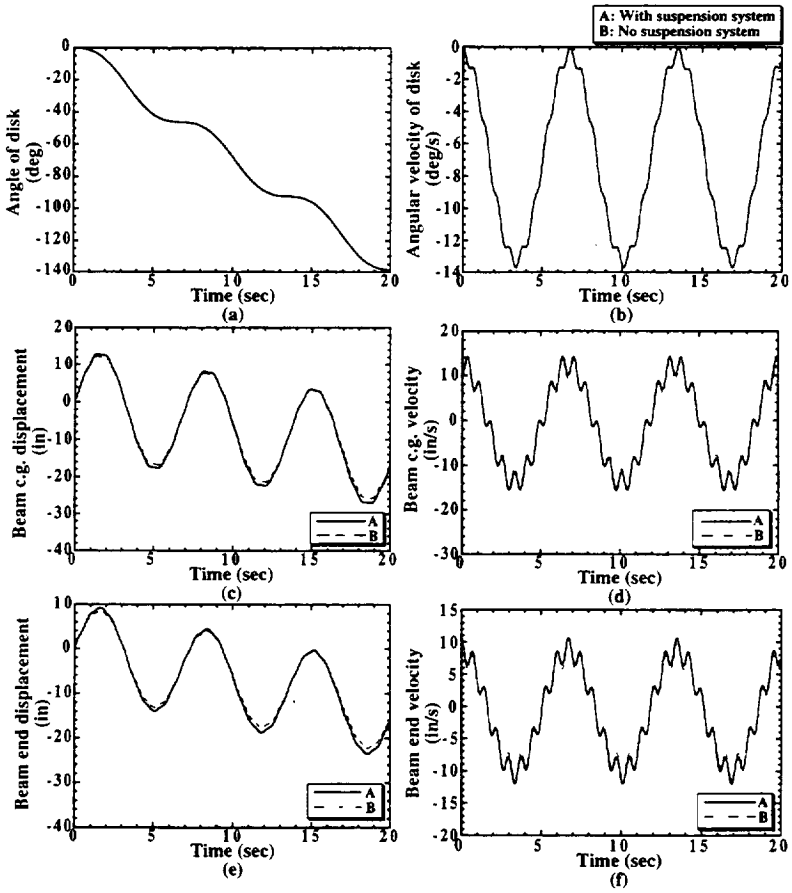

Fig. 10 Simulation results of a flexible steel beam for the excitation of the initial velocity

mass-spring system as a lumped-parameter model, and a flexible steel beam as a continuous parameter system. The lumped-parameter element is composed of two masses and a connecting spring which provides a single-mode vibration. Simulation results indicate that the characteristics of the flexible space structures can be precisely tested under this disk suspension system. It has also shown to be capable of permitting a constant-speed motion superimposed with flexural vibration in an impulse response. These simulation results provide very useful insights in building an experimental setup at NASA Langley.

Acknowledgments

The first and second authors wish to acknowledge the support of this investigation through NASA Grant No. NAG1-830 from NASA Langley Research Center.

References

1 Yang, L.-F., Chew, M., and Juang, J.-N., 1990, "Ground-Based Testing of the Dynamics of Flexible Space Structures Using Band Mechanisms," *Proceedings of the 1990 ASME Design Technical Conference*, Chicago, IL, DE-Vol. 24, pp. 143–152.

2 Chen, F. Y., 1982, *Mechanics and Design of Cam Mechanisms*, Pergamon Press, New York.

3 Greenwood, D. T., *Principles of Dynamics*, Prentice-Hall, Inc., Englewood Cliffs, NJ.

4 Meirovitch, L., 1971, *Analytical Methods in Vibrations*, Third Printing, MacMillan Company, New York, NY.

5 Huang, J.-K., Yang, L.-F., and Juang, J.-N., 1988, "Large Planar Maneuvers for Articulators Flexible Manipulators," *Proceedings of the Guidance, Navigation and Control Conference*, AIAA paper No. 88-4119, August.

6 Juang, J.-N., Yang, L.-F., and Huang, J.-K., 1989, "Lyapunov-based Control Designs for Flexible-Link Manipulators," AIAA/ASME/ASCE/AHS 30th Structures, Structural Dynamics and Materials Conference, AIAA 89-1214, Mobile, AL, April 5-7.